Nonlinear Dynamics of Quantum Cascade Laser in Ring Cavity

A THESIS
SUBMITTED TO THE FACULTY OF THE GRADUATE SCHOOL
OF THE UNIVERSITY OF MINNESOTA
BY

HADI MADANIAN

IN PARTIAL FULFILLMENT OF THE REQUIREMENTS
FOR THE DEGREE OF
MASTER OF SCIENCE

Adviser: Prof. Jing Bai

June 2011

Acknowledgements

I would like to thank my research adviser, Prof. Jing Bai, for her endless help and support during this thesis. I learned a lot from her during this work.

My appreciation also goes to Prof. Michael Sydor and Prof. Jonathan Maps for serving on my thesis defense committee.

I also want to thank the help from Prof. Alec Habig, who was previously the Director of Graduate Studies in the Physics Department.

Abstract

Quantum cascade lasers are of great interest because of their working range and high output power. Many investigations about these lasers are being done both experimentally and theoretically and part of the experimental work is mainly concerned with the confirmation of theoretical predictions. On the theory part, simulating the laser operation demands many mathematical approximations and physical interpretations. To a very good extent, results of the simulation conform to the experiment. Incorporating nonlinear effects to the QC lasers makes them even more interesting as it becomes easier to go beyond the level of performance and limitations dictated by the materials of the laser.

In this thesis, we tried to understand the effect of nonlinearity on propagation of a pulse inside the medium of the laser. Specifically, we looked at saturable absorber (SA) effect on the propagation of pulse. Saturable absorber is the basis of some other major nonlinear effects as well. A finite difference approximation (up to second order truncation error) was used to numerically solve the Maxwell-Bloch equations with SA term and graphs were produced to compare the shape of the wave with and without the influence of SA.

Table of Contents

List of Figures

CHAPTER 1

Introduction

1.1. Overview of Development of Quantum Cascade Lasers

First semiconductor laser was invented in 1962 and shortly after Kramer invented the Double Heterostructure Laser (DHLs) in 1963. In the DHL the active region is sandwiched by semiconductors of larger bandgap which results in carrier confinement and laser light is generated based on stimulated emission. The Quantum Well (QW) laser was invented in 1974 by Dingle and Henry in which the active region is a DHL with stacked quantum wells. Another improvement was made to semiconductor lasers in 1990 by introducing the Vertical Cavity Surface Emitting Lasers (VCSELs) in which the laser beam propagates perpendicular to the top surface or QWs plane. The Quantum-dot (QD) lasers are also in the category of semiconductor lasers but they exhibit performance that is close to gas lasers, and that's due to the tight confinement of the electron in quantum dots which resembles a structure similar to atoms. Temperature insensitivity is the main characteristic of this laser. The level of manufacturing sophistication has been increasing through the years parallel to the new developments in semiconductor technology and specifically crystal growth [1].

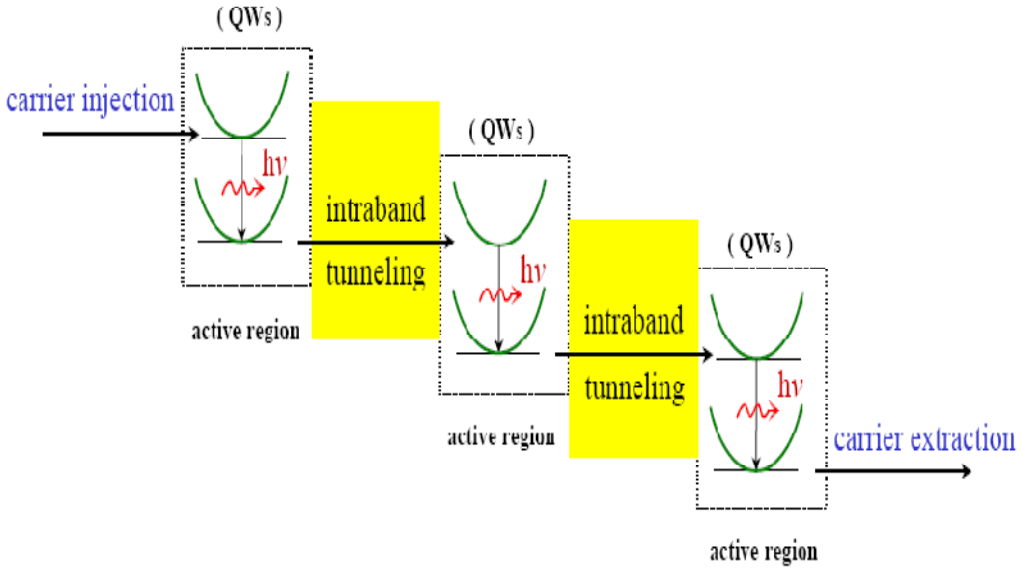

Figure 1-1 Conduction band energy diagram of Quantum Cascade Laser. The active regions where lasing occurs are shown with emitting photon and intersubbands and transition regions are marked with yellow.

The first experimental demonstration of a Quantum Cascade laser (QCL) was performed by Faist *et al* in 1994 with 4.3 μm wavelength only at cryogenic temperatures [2]. Since then, the lasers' performance has greatly improved. For instance, operation spanning the mid- to far-infrared (wavelength range from 3.5 to 24 μm), peak power levels in the watt range, and above room temperature (RT) pulsed operation for wavelengths from 4.5 to 16 μm are some of the major improvements.

Quantum cascade lasers take advantages of superlattice structures to construct conduction bands for electron transition. Unlike semiconductor diode lasers, which work based on electron transition between the valence band and conduction band and gas lasers which rely on population inversion between two energy levels in atom, the formation of laser light in QCLs is based on the transition of electrons between discrete energy states inside the conduction bands. QCLs are compact and high power light sources that can

operate in single or multi-mode, pulsed or continuous wave mode. By using band gap engineering, QCLs can be design to emit light at any wavelength in a broad energy range and this range is determined by the fundamental properties (e.g. band gap) of the material system of the superlattice [1].

1. 2. Band Engineering of Quantum Cascade Lasers

Designing QCLs is therefore a sophisticated process in band-structure engineering which is a powerful technique that allows building band diagrams with arbitrary and continuous band-gap variations. This lets QCL designers tune the transport properties of electrons and holes independently and continuously. From the quantum mechanics point of view, the energy states that electrons can occupy take a quantized form in the periodic potential structure. Solving the Schrödinger equation with this periodic potential for electrons results in a set of discrete allowed states for electrons in a semiconductor. And since there are stacks of different semiconductors in devices like QCLs, it's even more complicated to calculate the path of an electron in the device. These properties stem from the position of conduction and valence bands of the material which, depends on the concentration of electrons. The concentration of electrons is determined by the materials that were used in growing the device. Band-structure engineering combined with molecular beam epitaxy (MBE) has played a key role in the invention and development of many modern semiconductor devices and materials with tunable electronic and optical properties. Molecular beam epitaxy is a crystal growth technique capable of depositing thin films down to a thickness of one molecular layer. Fabricating QCLs for instance,

requires MBE with sophisticated band-gap calculation of the material system [3]. In an MBE machine different materials are deposited layer by layer and the thickness of the layers can be controlled down to single atom per layer. A diagram of this machine is shown in figure 1-2.

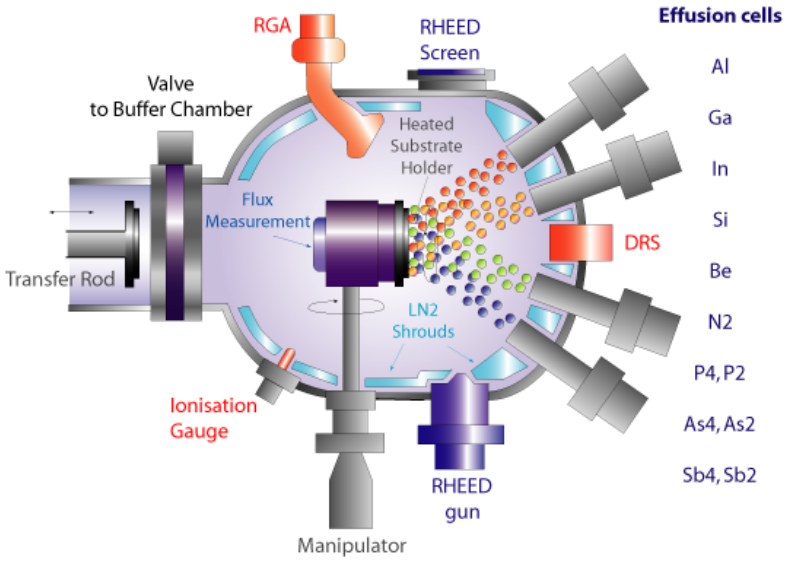

Figure 0-2 Diagram of MBE[20].

In the recent years, some improvements have been made to several types of material systems composing QCL structures. By using liquid nitrogen cooled environment, the GaAs/AlGaAs material system can emit beyond 13 μm with maximum working temperature of 230 K [2]. This improvement is done through better design of the active region through three-well vertical transition active region, better injection efficiency with funnel injectors and low doping concentration in the injector and using InP cladding layer to optimize the heat dissipation[4]. The working temperature in many designs is important. For example in long-wavelength QC lasers, the frequency is small due to the long wavelength of the pulse, which means that the separation between the

states must be small so that the transition of electron releases lower frequencies. A small gap between the states makes the laser vulnerable to thermal excitation. A small increase in the temperature causes the electrons to leave the states and disturb the population inversion. However, the working temperature cannot be too low (e.g. cryogenic temperatures) if the laser is to be used in wide range of applications.

Although, semiconductors lasers serve in many purposes, QCLs have made them obsolete in many applications. The major differences between the conventional semiconductor lasers and QCLs stem from the structure of the band gap. Some of the major differences are listed in the table below.

Conventional Laser	**Quantum Cascade Laser**
Holes and electrons are exhausted at each emission	Electrons are reused several times for photon emission
Both electrons and holes are needed for lasing (bipolar device)	Only electrons do the transition and emit photons (unipolar device)
Photon emission relies transition between conduction and valence band	Photon emission relies on intraband transitions between quantized conduction band states in quantum wells.
Wavelength depends on the material's band gap.	Wavelength depends on the size of the quantum wells and super lattices

Table 1-1 Comparison between QCLs and conventional semiconductor lasers.

1.3. Various Designs of Quantum Cascade Lasers

There are several design types to QCLs. Fabry-Perot (FP) QCLs are made of optical waveguide with material system of quantum cascade and with two ends of the waveguide cleaved to form the Fabry-Perot (FP) resonator. So the medium of the laser is the medium in which the pulse propagates through. Fabry-Perot quantum cascade lasers can emit multimode pulses and the frequency of the pulse depends on the temperature. Ring cavity QCLs on the other hand, consist of a circular lasing medium and laser pulses go through a circular motion.

The distributed feedback (DFB) QCL is explained in reference [5] in which a grating is incorporated in the structure of the laser. This feature enables the laser to operate above room temperature in the pulsed single mode with high peak power. The distributed feedback QCLs are fabricated in two different ways: First approach is the top-grating which is easier to build, and second approach is the buried-grating with epitaxial regrowth, which generally has a greater single-mode output as a result of larger coupling factor [6]. The coupling factor quantifies the amount of coupling between the forward and backward traveling waves in the cavity of DFB lasers [7]. Because of high optical power, room-temperature operation, and narrow intrinsic line width, QC-DFB lasers are excellent choices as narrow-band light sources in mid-infrared trace gas sensors [6]. In fact for gas sensing spectroscopy, the laser has to operate with stable single-mode emission and controlled tunability. By using techniques such as, tunable infrared laser diode absorption (TILDA) spectroscopy and knowing the finger print of gasses, it is possible to detect a specific gas of interest in a medium (e.g. in the atmosphere)[1]. In

reference [8] two types of DFB-QC lasers are proposed to meet the aforementioned aims. ‘‘Loss-coupled’’ devices, emitting at λ_{em}=55.4 and 7.8 μm, with a metal-semiconductor grating etched into the top surface of the device, and ‘‘index-coupled’’ lasers at λ_{em}=55.4 μm with the grating located directly above the active material. Three distinct designs of the active region, the so-called ‘vertical’ and ‘diagonal’ transition as well as the ‘superlattice’ active regions have emerged and are used either with conventional dielectric or surface plasmon waveguides. Fabricated as distributed feedback lasers, they provide continuously tunable single-mode emission in the mid-infrared wavelength range. This feature together with the high optical peak power and RT operation makes QC-lasers a prime choice for narrow-band light sources in mid-infrared trace gas sensing applications. Finally, a manifestation of the high-speed capabilities can be seen in actively and passively mode-locked QC-lasers, where pulses as short as a few picoseconds with a repetition rate around 10 GHz have been measured [8].

One of the most interesting applications of QCLs is in the terahertz spectrum (a frequency range defined approximately as the frequencies from 300 GHz to 10 GHz, or the wavelengths from 30 μm to 1000μm). Terahertz QCLs were first introduced by Köhler *et al.* [19] at the Scuola Normale Superiore in Pisa, Italy with pulse wavelength of 67 μm. Currently, the range of the laser spectrum is from 0.84-5.0 THz at a maximum temperature up to 169K in pulsed mode and 117K in continuous wave mode and output powers of up to 250 mW in pulsed mode and 130 mW in continuous modes although these figures are not from the same device. This great performance of QCLs arises from the fact that they radiate below the longitudinal-optical phonon energy. Besides, other

sources, like gas lasers or free electron lasers have limited output power, require extensive cryogenic cooling or are not efficient in size or cost. However, it appears that generating long-wavelengths is more difficult than the mid-infrareds in QC laser for two reasons. First, because terahertz photon energies are small, it's difficult to selectively inject or remove electrons by tunneling or scattering from such closely spaced subbands to achieve the population inversion necessary for gain. Second, as losses due to the absorption of radiation increases proportionally to the square of the wavelength, waveguides are required so that minimize the modal overlap with any doped semiconductor layers [9].

1.4. Dynamic Behavior of Quantum Cascade Lasers

The dynamics of QCLs is controlled by the ultrafast carrier lifetime in these devices (on the order of picoseconds) and this lifetime is determined mainly by the quantum well structure [1]. The carrier lifetime is the time that it takes to transit from one active region of the laser to the next. The combination of optical nonlinearities and ultrafast dynamics is one of the major characteristics of QCLs. Self-Mode-Locking is used in lasers to generate optical pulses with duration in the picoseconds and femtoseconds range. The origin of Self-Mode Locking is due to the transverse Kerr lensing mechanism in the lasing medium. Based on equation (1.4), if the nonlinear refractive index is positive, the total refractive index increases with the intensity. Any peak of the beam has a higher intensity than the edges and as a result has higher refractive index. This leads to an increase of the beam confinement at the center and the

beam diameter becomes narrower. This effect is known as Kerr lensing effect. In mode-locking technique, the longitudinal modes of the laser cavity are locked in phase, by some external or internal mechanisms, to produce a train of pulses with ultrashort duration and repetition rate equal to the cavity roundtrip frequency. Self mode-locking of QC lasers with large optical nonlinearities is explained in reference [12], in which the intensity-dependent refractive index of the lasing transition creates a nonlinear wave guide where the optical losses decreases with increasing intensity. This nonlinear effect prepares the system for generation of ultrashort pulses.

Since QCLs generate short pulses, both nonlinear and dispersive effects of the medium of the laser influence their shape and spectra. These effects arise from the fact that both electrons and nuclei respond to high intensity electric field in a different way that they do to a low intensity field. The wave equation for propagating pulse inside the cavity of laser is given by:

$$\nabla^2 E - \frac{1}{c}\frac{\partial^2 E}{\partial t^2} = \mu_0 \frac{\partial^2 P_L}{\partial t^2} + \mu_0 \frac{\partial^2 P_{NL}}{\partial t^2} \qquad (1.1)$$

where P_L and P_{NL} are the linear and nonlinear polarization of the medium. The linear and nonlinear parts of the polarization are related to the electric field $E(r,t)$ [13, p.31]. In this equation P_{NL} is treated as a small perturbation to P_L. In this case, TM polarized electric field and components of polarization can be written in the form of:

$$\vec{E}(r,t) = \frac{1}{2}[E(r,t)e^{-i\omega_0 t} + c.c.]\hat{x} \qquad (1.2.a)$$

$$\overrightarrow{P_L}(r,t) = \frac{1}{2}\left[P_L(r,t)e^{-i\omega_0 t} + c.c.\right]\hat{x} \qquad (1.2.b)$$

$$\vec{P}_{NL}(r,t) = \frac{1}{2}\left[P_{NL}(r,t)e^{-i\omega_0 t} + c.c.\right]\hat{x} \qquad (1.2.c)$$

$\hat{x}$ direction is selected as any arbitrary direction perpendicular to the direction on propagation of wave (in this case $\hat{z}$) and dielectric constant of the medium is also frequency dependent with nonlinear part;

$$\varepsilon(\omega) = 1 + \chi^1(\omega) + \varepsilon_{NL} \qquad (1.3)$$

where χ is called the susceptibility of the medium. The dielectric constant can be used to define the refractive index $\tilde{n}$ and the absorption coefficient $\tilde{\alpha}$ which both become intensity dependent because of ε_{NL};

$$\tilde{n} = n + n_2|E|^2 \qquad (1.4)$$

$$\tilde{\alpha} = \alpha + \alpha_2|E|^2 \qquad (1.5)$$

n is the linear refractive index which is the ratio of velocity of light in the vacuum to the velocity of light in the medium. n_2 and α_2 are nonlinear-index coefficient and two-photon absorption coefficient respectively.

1.5. Motivation

There are many giant optical nonlinearities influencing the propagation of pulse in the medium of the QCLs. Self-phase-modulation, self-mode-locking and saturable absorber effects that will be reviewed in the next chapter are manifestations of the nonlinearity in the medium of the laser. These effects give rise to extraordinary changes in the pulse while passing through the medium of the laser. Our research is focused on

understanding the evolution of a pulse inside the nonlinear medium of a QCL with and without nonlinear effects. We try to understand how the shape of the pulse changes under different circumstances and how the equations describing the physics of light propagation change in each case. Some approximations were used in deriving the equations to make them easier to solve and we will consider consistency in the results with the experimental results and also previously existing simulations. We are specifically interested in investigating the effect of saturable absorber in the medium because of its importance in generating ultrashort pulses and mode-locking and Q-switching in lasers.

Thesis is organized as follows: The development and progress of QC lasers is discussed in Chapter One. Required theoretical background is provided in Chapter Two. Working principles of Saturable Absorber and Self-Phase Modulation effects are described. In Chapter Three, formalism of light propagation is explained and different ways of writing the equations for dynamic of pulse is presented. Finite difference approach to model the equations is used and included in this chapter. The conversion coefficients between the equations without the nonlinear effect and with the nonlinear effect are also given in Chapter Three. In Chapter Four, the results of the simulation are presented and the different graphs that we generated are pictured. And finally in Chapter Five, we discuss the results and compare them with other experimental and theoretical results.

CHAPTER 2

Theoretical Background

2.1. QCL Working Principles

Quantum cascade lasers are different fundamentally from other semiconductor lasers. This difference has been made clear in figure 2-1. QCLs are made up of quantum semiconductor structures known as quantum wells. Based on the solution to Schrödinger equation, discrete energy levels are formed inside the quantum wells and electrons can tunnel to the adjacent well if the thickness of the barrier is small enough. As a result of this tunneling and diffusion of wave functions, minibands are formed within the array of quantum wells. This structure is pictured in figure 2-2.

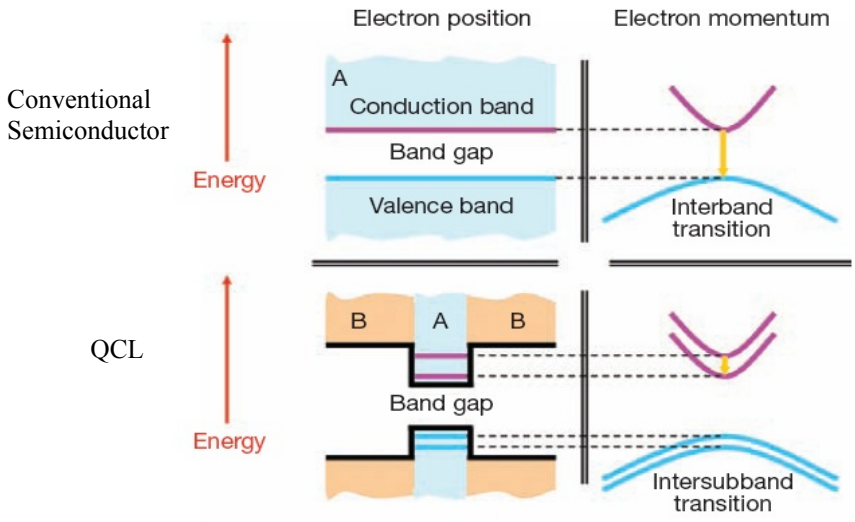

Figure 2-1 QCLs and conventional semiconductors energy diagrams.

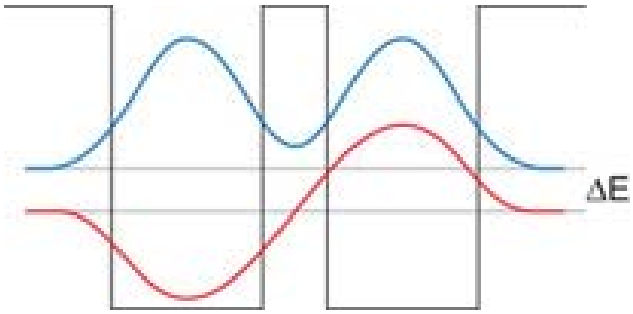

(a)

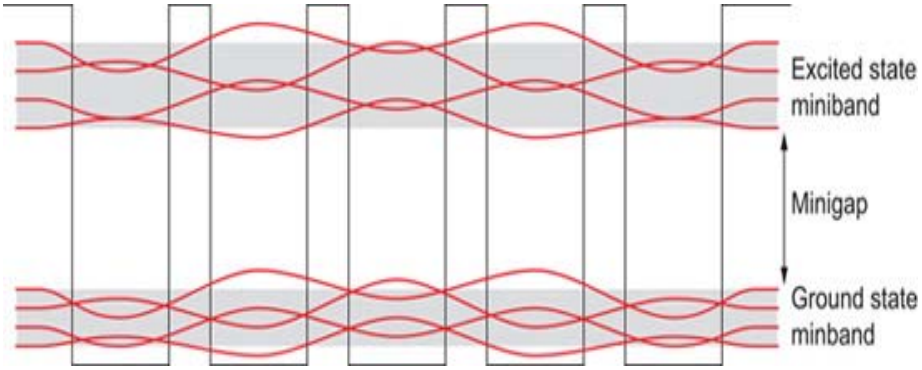

(b)

Figure 2-2 (a) Tunneling of electrons and diffusion of wave functions. (b) The minibands are formed in the array of quantum wells.

Different regions can be distinguished in QCLs. The active region and injector region. The active region is the place where electrons do transitions between intersubbands (minibands) and emit photons and then they can tunnel through the injector to enter the next active region. Upon applying an electric potential to the system, electrons can stream down the superlattice, which now has a potential gradient, and sequentially emit photons. Population inversion, which is necessary part of the lasing process, is achieved by the controlled tunneling of electrons. Since the thickness of the different layers determines the rate of tunneling and also the wavelength of the emitted photon, band-structure engineering is the key to design the superlattice structure. The working range of quantum

cascade lasers is in mid-infrared and because of cascading of electrons and emitting photons at different steps the output power of this type of laser is higher than other semiconductor lasers [1].

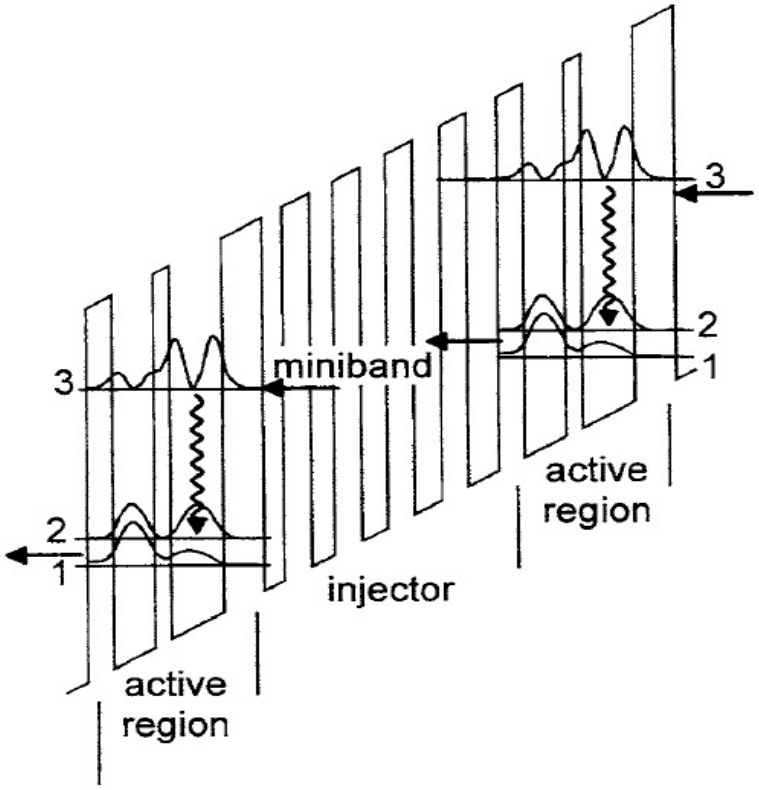

Figure 0-3 Conduction band diagram. Two active regions with intermediate injector are indicated. The laser transition is shown by the wavy arrow (from 3 to 2) [1].

2.2. Ring Laser Cavity

All laser cavities (resonators) share two characteristics that complement each other: (1) they are basically linear devices with one relatively long optical axis, and (2) the sides perpendicular to this axis are open. In the case of ring lasers the long axis actually bends and closes on itself [14]. There is no standing wave formed in ring lasers

because of lack of reflectors at two ends so we don't see spatial hole burning (SHB) effect in the ring laser for which the standing wave is a requirement. In FP cavity however, laser pulses go back and force between two coparallel reflecting plates which makes the existence of standing wave possible. We will consider QCL structures as a ring laser and light pulses can go around a loop in the cavity of laser. As shown in the figure below, the laser light comes out of the device and then it is directed by a set of mirrors to a ring shape.

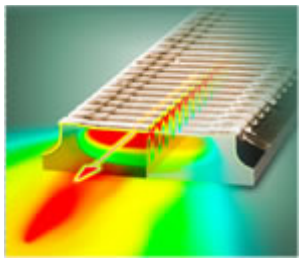

(a)

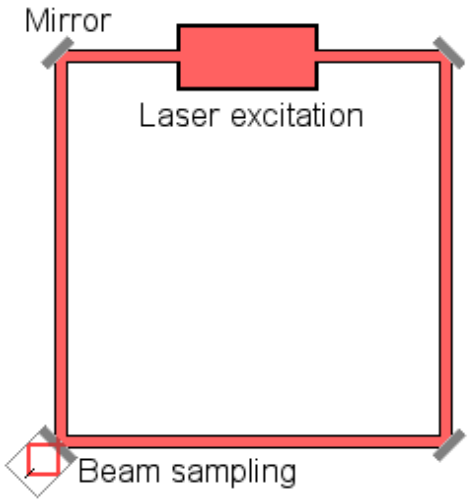

(b)

Figure 2-2 (a) The direction of pulse output from stacks of quantum wells. (b) Schematic diagram of ring cavity laser. Pulses go around a loop

2.3. Self-Phase Modulation

This effect is considered to originate from the optical nonlinear Kerr effect, which is a change in the refractive index of materials in response to an electric field passing

through them. The intensity dependence of the refractive index leads to a large number of interesting nonlinear effects. Self-phase modulation refers to the self-induced phase shift experienced by an optical field during its propagation in the medium. Magnitude of SPM can be obtained by knowing the fact that the phase of an optical pulse changes by:

$$\emptyset = (n + n_2|E|^2)k_0 L \tag{2.1}$$

where k_0 is the wave-vector of the pulse and L is the cavity length, n is the linear part of the refractive index and n_2 is the nonlinear index coefficient. From this equation, intensity-dependent nonlinear phase shift, $\emptyset_{NL} = n_2|E|^2 k_0 L$, is due to SPM. Among other effects, SPM is responsible for spectral broadening of ultrashort pulses and formation of optical solitons in the cavity. Self-phase-modulation was first observed in 1967 in the context of transient self-focusing of optical pulses propagating in CS_2 cells [15].

2.4. Saturable Absorber

A saturable absorber is an optical material or component in which the absorption decreases with incident optical intensity. So with increasing intensity, absorption saturates, loss decreases, and the transmittance increases. The effect of saturable absorbption can be simulated by Kerr-focusing: the high intensity part of the beam is focused by the Kerr-effect, whereas the low intensity parts remain unfocused. If this pulse is passed through a device, the low intensity parts are weakened and as a result pulse is shortened [15]. Several types of processes contribute to a semiconductor saturable absorber. The most straight forward mechanism in a saturable absorber is

caused by the dependence of the absorption coefficient on the carrier population in the saturable absorber material. Mainly in quantum wells and bulk materials, where we have slow saturable absorption, this is usually quantified by the simple approximation for the saturable absorption coefficient and is measured experimentally. We show this coefficient by $\boldsymbol{\gamma}$.

A saturable absorber can be used as an optical switch to suppress low-intensity signals in favor of short and intense optical pulses. Or, it can be implemented to facilitate or enhance the mode locking of lasers.

Saturable absorber may have two main geometries. The first that is used in semiconductor lasers and integrated optical circuits is the waveguide saturable absorber and the other construction is semiconductor saturable absorber mirror (SESAM) that is used as a saturable reflector.

2.5. Maxwell-Bloch Formalism for Ring Cavity

The initial equations are the laser matter equations and Maxwell's equations. In Maxwell's equations the effect of a material is usually described by the polarization of the medium. The matter equations determine the polarization under the influence of an electric field E. The same concept can be applied to the active atoms of a laser. If we assume that the active material of the laser consists of two-level atoms, the laser matter equations for the polarization per unit volume P and for the population inversion, which is difference between the number of electrons in two levels, of the two-state system per unit volume S are given by [16]:

$$\ddot{P} + 2\gamma_{\perp}\dot{P} + {\omega_0}^2 P = -\frac{2}{3}\left(\frac{|M|^2}{\hbar}\right)\omega_0 ES \tag{2.2}$$

$$\dot{S} = \gamma_{\parallel}(d_0 - S) + \left(\frac{2}{\hbar\omega_0}\right)P.E \tag{2.3}$$

In these equations, $\gamma_{\perp}$ describes the damping of the polarization, M is the optical dipole matrix element, $\gamma_{\parallel}$ is the relaxation constant of the population inversion and d_0 is the pumping, and $\hbar\omega_0$ is the energy separation between the states. These equations can be derived from the two-level Schrodinger equation of density matrix equations. Maxwell's equations together with matter equations and periodic boundary conditions describe the effect of an active material in a medium of the laser.

$$\vec{\nabla} \times \vec{H} = P + \epsilon\dot{E} + 2\epsilon kE \tag{2.4.a}$$

$$\vec{\nabla} \times \vec{E} = -\mu\dot{H} \tag{2.4.b}$$

$$\vec{\nabla}.(\epsilon E + P) = 0 \tag{2.4.c}$$

$$\vec{\nabla}.H = 0 \tag{2.4.d}$$

where, k determines the loss of the medium (in this case ring cavity), ϵ and μ are susceptibility and permeability respectively. Now, if we apply the equations (2.2)-(2.4) to a one-dimensional ring laser by assuming that the field vectors are polarized perpendicularly to the laser axis, x, and eliminate the magnetic field H using Maxwell's equations the one-dimensional wave equation:

$$\frac{\partial^2 E_y}{\partial x^2} - \left(\frac{1}{c^2}\right)\frac{\partial^2 E_y}{\partial t^2} - \left(\frac{2k}{c^2}\right)\frac{\partial E_y}{\partial t} = \mu\frac{\partial^2 P_y}{\partial t^2} \tag{2.5}$$

where $c = \frac{1}{\sqrt{\mu\epsilon}}$ is the velocity of light in the host material. The boundary conditions of ring laser require that P_y, E_y, and S be periodic in x with period L;

$$P_y(x + L, t) = P_y(x, t) \tag{2.6.a}$$

$$E_y(x + L, t) = E_y(x, t) \tag{2.6.b}$$

$$S(x + L, t) = S(x, t) \tag{2.6.c}$$

where L is the length of the cavity.

To be able to find a solution for these equations, without disturbing the physics of the problem, we use rotating wave approximation which implies that $\tilde{E}$, $\tilde{P}$ and $\tilde{S}$ are slowly varying functions of x (with respect to the wavelength $\lambda = \frac{2\pi c}{\omega_0}$ of the emitting photon) and t (with respect to the period $T = \frac{2\pi}{\omega_0}$ of the emitting photon). So in the ring cavity when propagation is in one direction we have:

$$E_y = \tilde{E}(x, t)e^{i\omega_0\left(\frac{x}{c} - t\right)} + c.c \tag{2.7.a}$$

$$P = \tilde{P}(x, t)e^{i\omega_0\left(\frac{x}{c} - t\right)} + c.c. \tag{2.7.b}$$

$$S = \tilde{S}(x, t) \tag{2.7.c}$$

by using this approximation, we can neglect second-order derivatives in the slowly varying functions of $\tilde{E}_y$, $\tilde{P}_y$ and $\tilde{S}$ and obtain finally the following equations:

$$\dot{\tilde{P}} + \gamma_{\perp}\tilde{P} = -\left(\frac{i}{3}\right)\left(\frac{|M|^2}{\hbar}\right)\tilde{E}\tilde{P} \tag{2.8}$$

$$\dot{\tilde{S}} = \gamma_{\parallel}(d_0 - S) + \left(\frac{2i}{\hbar}\right)(\tilde{E}\tilde{P}^* - \tilde{E}^*\tilde{P}) \tag{2.9}$$

$$c\frac{\partial\tilde{E}}{\partial x} + \dot{\tilde{E}} + k\tilde{E} = \left(\frac{\omega_0}{2\epsilon}\right)i\tilde{P} \tag{2.10}$$

for more simplicity we limit the variables to the case where k, c and d_0 are independent of x, which means the medium is homogeneous in loss and gain distribution. with a new set of boundary conditions:

$$\tilde{P}(x + L, t)e^{i\omega_0\left(\frac{L}{c}\right)} = \tilde{P}(x, t) \tag{2.11.a}$$

$$\tilde{E}(x + L, t)e^{i\omega_0\left(\frac{L}{c}\right)} = \tilde{E}(x, t) \tag{2.11.b}$$

$$\tilde{S}(x + L, t) = \tilde{S}(x, t) \tag{2.11.c}$$

For more simplicity we limit the variables to the case where k, c and d_0 are independent of x, which means the medium is homogeneous in loss and gain distribution. And also we assume that one cavity mode is in resonance with frequency ω_0, so $e^{i\omega_0\left(\frac{L}{c}\right)} = 1$ and the new boundary conditions are:

$$\tilde{P}(x + L, t) = \tilde{P}(x, t) \tag{2.12.a}$$

$$\tilde{E}(x + L, t) = \tilde{E}(x, t) \tag{2.12.b}$$

$$\tilde{S}(x+L,t) = \tilde{S}(x,t) \tag{2.12.c}$$

By using the reduced quantities:

$$E = \frac{\tilde{E}}{\tilde{E}_{cw}}$$

$$P = \frac{\tilde{P}}{\tilde{P}_{cw}} \tag{2.13}$$

$$\sigma = \frac{\tilde{S}}{\tilde{S}_{cw}}$$

$$\lambda = \frac{(d_0 - \tilde{S}_{cw})}{\tilde{S}_{cw}}$$

where λ is called the normalized pumping parameter and the cw indices refer to normalized to stationary (continuous wave) and independent of x and t solutions. Then equations (2.8) reduce to the following equations:

$$\dot{P} + \gamma_{\perp} P = \gamma_{\perp} \sigma \tag{2.14}$$

$$\dot{\sigma} + \gamma_{\parallel} \sigma = \gamma_{\parallel} [1 + \lambda - \frac{1}{2} \lambda (E^* P + P^* E)] \tag{2.15}$$

$$\dot{E} + \frac{c}{n} \frac{\partial E}{\partial x} = k(P - E) \tag{2.16}$$

In deriving the above equations Rotating Wave Approximation (RWA) was used which is based on the assumption that the counterrotating wave terms (harmonics of electrics field and polarization oscillations with frequencies higher than resonant frequency) can be neglected [17]. Equation (2.14) is the rate of change in the

polarization. Equation (2.15) explains the rate of change in the population inversion and equation (2.16) defines the evolution of the electric field of the pulse in the medium.

Another way of deriving the Maxwell-Bloch equations in a ring cavity is by modeling the gain medium of the laser as a two-level system described by Bloch equations. The equation for electric field, polarization and inversion inside the ring cavity with the effect of saturable absorber is given by [18]:

$$\frac{\partial \tilde{E}}{\partial t} + \frac{c}{n}\frac{\partial \tilde{E}}{\partial z} = -\frac{c}{n}\tilde{P} - \left(\frac{1}{2}l_0^{'} - \gamma\left|\tilde{E}\right|^2\right)\tilde{E} \tag{2.17}$$

$$\frac{\partial \tilde{P}}{\partial t} = -\frac{1}{2}\tilde{\sigma}\tilde{E} - \frac{\tilde{P}}{T_2} \tag{2.18}$$

$$\frac{\partial \tilde{\sigma}}{\partial t} = \frac{l_0 p}{T_1 T_2} - \frac{\tilde{\sigma}}{T_1} + (2\tilde{E}^*\tilde{P} + c.c.) \tag{2.19}$$

The SA effect is characterized by γ and $l_0^{'}$ is the linear loss. T_1 and T_2 are the longitudinal and transverse relazation times respectively. In deriving these equations, slowly varying envelope approximation (SVEA) is used in which we assume that the envelope of the pulse varies slowly in time and space compared to …. Because of the similarities between equations (2.17)-(2.19) and the equations (2.14)-(2.16), we can find the conversion relations between the two sets which will help us in simulating the equations.

CHAPTER 3

Dynamics Analysis of Quantum-Cascade Laser in Ring-Cavity

3.1. Finite Difference Approximation to Maxwell-Bloch Equations for Ring-Cavity with Vacuum Medium

As explained in chapter 2, Maxwell-Bloch equations describe the dynamics of a simple two level laser. We follow the derivation presented in Ref. [16]. Starting with equation set (2.14-2.16):

$$\dot{P} + \gamma_{\perp} P = \gamma_{\perp} \sigma$$

$$\dot{\sigma} + \gamma_{\parallel} \sigma = \gamma_{\parallel} [1 + \lambda - \frac{1}{2} \lambda (E^* P + P^* E)]$$

$$\dot{E} + c \frac{\partial E}{\partial x} = k(P - E)$$

In these equations, E represents the electric field, P is the polarization of the medium and σ is population inversion, $\gamma_{\perp}$ and $\gamma_{\parallel}$ damping of the polarization and relaxation constant of the population inversion respectively. Since we focus on the real part of the polarization and electric field, therefore $E^* = E$ and $P^* = P$. Equations (2.14)-(2.16) then can be written in the new form:

$$\dot{P} + \gamma_{\perp} P = \gamma_{\perp} \sigma E \tag{3.1}$$

$$\dot{\sigma} + \gamma_{\parallel}\sigma = \gamma_{\parallel}[1 + \lambda - \lambda(EP)] \tag{3.2}$$

$$\dot{E} + c\frac{\partial E}{\partial x} = k(P - E) \tag{3.3}$$

We use finite-difference method to find the evolution of electric field, polarization and population inversion in the cavity both in time and space. To meet that goal, we need to change the equations to discrete forms to be able to find the state of the system step by step based on the state of the system in one step before. We show the procedure for electric field and full form of equations for the two others.

we divide the $x - t$ plane into a $m \times n$ grid with spacing Δx and Δt in space and time respectively as in Figure 3-1. For the ring cavity, spatial spacing is $\Delta x = \frac{L}{m}$ and spacing in time is $\Delta t = \frac{\Delta x}{v} = \frac{Ln_{ref}}{mc}$. The spacing between the grid points was chosen fine enough to make sure there is not any uninspected variation inside the spacing. This was achieved by increasing the dimensions of grids (m and n) until we see consistency in the results. For the purpose of ring cavity we use periodic boundary condition which means that the red lines in figure 3-1 must be equal. The initial condition is also marked with purple line which is the state of the system at time zero and in the different positions in the ring.

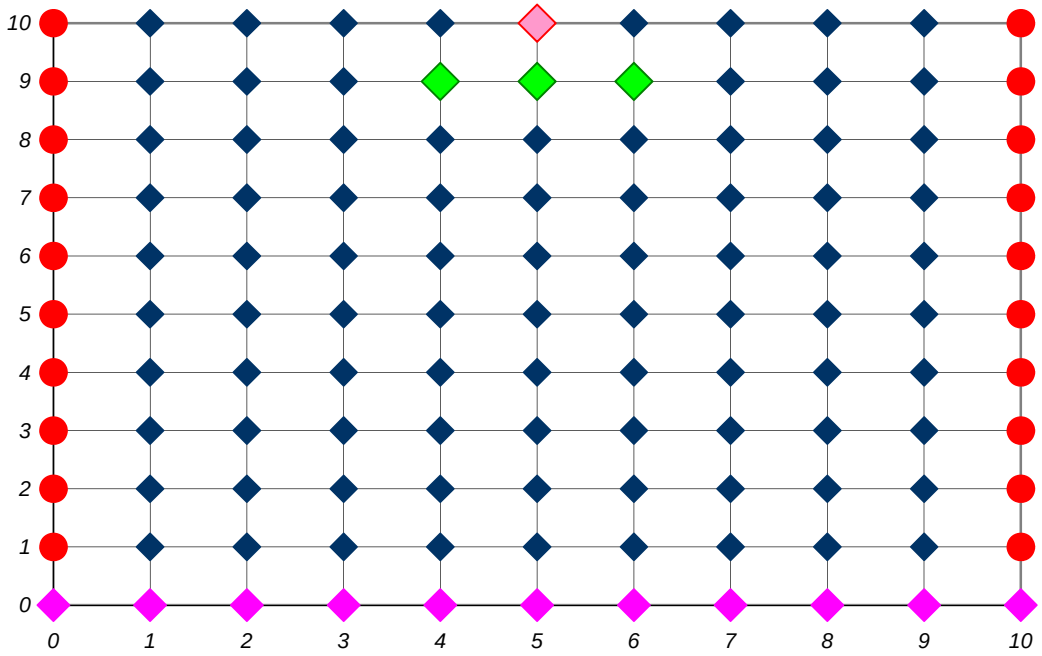

Figure 3-1 Simple mxn grid for finite difference approximation points. Here m=10 and n=10. The boundary conditions are shown by red dots and initial condition by purple dots. E(m,n+1) is shown with pink dot and its value is dependent on the values in previous steps, the green dots.

First we find the derivative of variables in time and space. This can be done by writing the Taylor expansion about the grid point (m, n).

$$\frac{\partial E}{\partial t} = \frac{E(m, n+1) - E(m, n)}{\Delta t} - \frac{1}{2}\Delta t \frac{\partial^2 E(m, n)}{\partial t^2} \tag{3.4}$$

$$\frac{\partial E}{\partial x} = \frac{E(m, n) - E(m-1, n)}{\Delta x} + \frac{1}{2}\Delta x \frac{\partial^2 E(m, n)}{\partial x^2} \tag{3.5}$$

as mentioned above, similar expressions can be written for $\frac{\partial P}{\partial t}$ and $\frac{\partial \sigma}{\partial t}$. Starting with the left-hand side of equation (3.3) for electric field we have:

$$\begin{aligned}\dot{E} + c\frac{\partial E}{\partial x} &= \frac{E(m,n+1) - E(m,n)}{\Delta t} - \frac{1}{2}\Delta t\frac{\partial^2 E(m,n)}{\partial t^2} \\ &\quad + \frac{E(m,n) - E(m-1,n)}{\Delta t} \\ &\quad + \frac{1}{2}c^2\Delta t\frac{\partial^2 E(m,n)}{\Delta x^2} \\ &= \frac{E(m,n+1) - E(m-1,n)}{\Delta t} \\ &\quad + \frac{1}{2}\Delta t\left[c^2\frac{\partial^2 E(m,n)}{\partial x^2} - \frac{\partial^2 E(m,n)}{\partial t^2}\right] \\ &\quad = k(P-E)\end{aligned} \tag{3.6}$$

here, selecting the second equality helps us to eliminate the terms with first derivative;

$$\begin{aligned}k(P-E) &= \frac{E(m,n+1) - E(m-1,n)}{\Delta t} \\ &\quad + \frac{1}{2}\Delta t\left[c^2\frac{\partial^2 E(m,n)}{\partial x^2} - \frac{\partial^2 E(m,n)}{\partial t^2}\right]\end{aligned} \tag{3.7}$$

solving (3.7) for $E(m,n+1)$:

$$\begin{aligned}E(m,n+1) &= k\Delta t(P-E) \\ &\quad + \frac{1}{2}\Delta t^2\left[\frac{\partial^2 E(m,n)}{\partial t^2} - c^2\frac{\partial^2 E(m,n)}{\partial x^2}\right] \\ &\quad + E(m-1,n)\end{aligned} \tag{3.8}$$

the second derivatives are calculated by differentiating (3.3) and substituting the first order difference approximation from equations (3.2) and (3.1). In this way, we obtain an approximation to the derivatives with a truncation error of order $(\Delta t)^2$.

$$\frac{\partial^2 E(m,n)}{\partial t^2} = \ddot{E} = k\left(\dot{P} - \dot{E}\right) - c\frac{\partial^2 E}{\partial x \partial t} \tag{3.9}$$

$$\frac{\partial^2 E(m,n)}{\partial x^2} = \frac{k}{c}\left(\frac{\partial P}{\partial x} - \frac{\partial E}{\partial x}\right) - \frac{1}{c}\frac{\partial^2 E}{\partial x \partial t} \tag{3.10}$$

multiplying (3.9) by c^2 and subtracting it from (3.8):

$$\begin{aligned} &\frac{\partial^2 E(m,n)}{\partial t^2} - c^2\frac{\partial^2 E(m,n)}{\partial x^2} \\ &\qquad = k\left(\dot{P} - \dot{E}\right) - ck\left(\frac{\partial P}{\partial x} - \frac{\partial E}{\partial x}\right) \end{aligned} \tag{3.11}$$

we know:

$$\dot{P} = \gamma_\perp(\sigma E - P)$$

and

$$\dot{E} = k(P - E) - c\frac{\partial E}{\partial x}$$

then right-hand side of the equation (3.10) becomes:

$$\begin{aligned} &\frac{\partial^2 E(m,n)}{\partial t^2} - c^2\frac{\partial^2 E(m,n)}{\partial x^2} \\ &\qquad = k\left[\gamma_\perp(\sigma E - P) - k(P - E) + c\frac{\partial E}{\partial x}\right] \\ &\qquad + ck\left(\frac{\partial E}{\partial x} - \frac{\partial P}{\partial x}\right) \\ &= k[\gamma_\perp(\sigma E - P) - k(P - E)] + 2ck\frac{\partial E}{\partial x} - ck\frac{\partial P}{\partial x} \end{aligned} \tag{3.12}$$

$$= k[\gamma_\perp(\sigma E - P) - k(P - E)] + 2k\frac{E(m,n) - E(m-1,n)}{\Delta t}$$

$$- k\frac{P(m,n) - P(m-1,n)}{\Delta t}$$

$$= k[\gamma_\perp \sigma E - (\gamma_\perp + k)P + kE]$$

$$+ 2k\frac{E(m,n) - E(m-1,n)}{\Delta t}$$

$$- k\frac{P(m,n) - P(m-1,n)}{\Delta t}$$

where we used the following relationship for wave propagation in vacuum:

$$c = \frac{\Delta x}{\Delta t}$$

therefore evolution of electric field in time and space is given by:

$$\begin{aligned} E(m,n+1) = E(m-1,n) &+ k\Delta t(P - E) \\ &+ \frac{1}{2}\Delta t^2 k[\gamma_\perp \sigma E - (\gamma_\perp \sigma] + k)P + kE] \\ &+ k\Delta t[E(m,n) - E(m-1,n)] \\ &- \frac{1}{2}k\Delta t[P(m,n) - P(m-1,n)] \end{aligned} \tag{3.13}$$

rearranging the equation results in:

$$
\begin{aligned}
E(m,n+1) = {} & (1-k\Delta t)E(m-1,n) \\
& + \left(\frac{1}{2}k\Delta t - \frac{1}{2}k(\gamma_\perp + k)\Delta t^2\right)P(m,n) \\
& + \frac{1}{2}(k\Delta t)^2 E(m,n) + \frac{1}{2}k\gamma_\perp \Delta t^2 \sigma(m,n)E(m,n) \\
& + \frac{1}{2}k\Delta t P(m-1,n)
\end{aligned}
\tag{3.14}
$$

to avoid recalculating the constants and reduce the amount of calculations, equation (3.13) can be written as:

$$
\begin{aligned}
E(m,n+1) = {} & a_1 E(m-1,n) + a_2 P(m,n) \\
& + a_3 E(m,n) + a_4 \sigma(m,n)E(m,n) \\
& + a_5 P(m-1,n)
\end{aligned}
\tag{3.15}
$$

where

$$a_1 = (1-k\Delta t)$$

$$a_2 = \frac{1}{2}k\Delta t - \frac{1}{2}k(\gamma_\perp + k)\Delta t^2$$

$$a_3 = \frac{1}{2}(k\Delta t)^2$$

$$a_4 = \frac{1}{2}k\gamma_\perp \Delta t^2$$

$$a_5 = \frac{1}{2}k\Delta t$$

following a similar procedure for P and $\boldsymbol{\sigma}$ we have:

$$P(m,n+1) = b_1 P(m,n) + b_2 \sigma(m,n) E(m,n) + b_3 E(m,n) + b_4 \sigma(m,n) P(m,n) - b_5 P(m,n) E^2(m,n) + b_6 \sigma(m,n) E(m-1,n) \tag{3.16}$$

with the following coefficients:

$$b_1 = \left[1 - \gamma_\perp \Delta t + \frac{1}{2}(\gamma_\perp \Delta t)^2\right]$$

$$b_2 = \frac{1}{2}\gamma_\perp \Delta t[1 - (k + \gamma_\perp + \gamma_\parallel)\Delta t]$$

$$b_3 = \frac{1}{2}\gamma_\perp \gamma_\parallel \Delta t^2 (1 + \lambda)$$

$$b_4 = \tfrac{1}{2} k \gamma_\perp \Delta t^2 \quad , \quad b_5 = \tfrac{1}{2}\gamma_\perp \gamma_\parallel \lambda \Delta t^2 \quad , \quad b_6 = \tfrac{1}{2}\gamma_\perp \Delta t$$

and for population inversion we have:

$$\begin{aligned}\sigma(m,n+1) = {} & \sigma(m,n)\left[1 - \gamma_\parallel \Delta t + \frac{1}{2}(\gamma_\parallel \Delta t)^2\right] \\ & + P(m,n)E(m,n)\left[-\frac{1}{2}\lambda\gamma_\parallel \Delta t + \frac{1}{2}\Delta t^2 \lambda \gamma_\parallel (\gamma_\perp + \gamma_\parallel + \lambda)\right] \\ & + \sigma(m,n)E^2(m,n)\left[\frac{1}{2}\gamma_\parallel \gamma_\perp \lambda \Delta t^2\right] \\ & - P^2(m,n)\left[\frac{1}{2}\lambda k \gamma_\parallel \Delta t^2\right] \\ & - P(m,n)E(m-1,n)\left[\frac{1}{2}\lambda\gamma_\parallel \Delta t\right] + \gamma_\parallel \Delta t(1+\lambda)(1 \\ & - \frac{1}{2}\gamma_\parallel \Delta t)\end{aligned} \tag{3.17}$$

this is simply:

$$\sigma(m,n+1) = c_1\sigma(m,n) + c_2P(m,n)E(m,n) + c_3\sigma(m,n)E^2(m,n) - c_4P^2(m,n) - c_5P(m,n)E(m-1,n) + c_6 \tag{3.18}$$

where

$$c_1 = 1 - \gamma_\parallel \Delta t + \frac{1}{2}(\gamma_\parallel \Delta t)^2$$

$$c_2 = -\frac{1}{2}\lambda\gamma_\parallel \Delta t + \frac{1}{2}\Delta t^2 \lambda\gamma_\parallel(\gamma_\perp + \gamma_\parallel + \lambda)$$

$$c_3 = \frac{1}{2}\gamma_\parallel\gamma_\perp\lambda\Delta t^2$$

$$c_4 = \frac{1}{2}\lambda k\gamma_\parallel \Delta t^2$$

$$c_5 = \frac{1}{2}\lambda\gamma_\parallel \Delta t$$

using finite difference equations demands that we introduce initial conditions to the system. The initial condition for electric field is a simple Gaussian pulse according to the reference [16].

$$E(x,0) = 0.1e^{-100(\frac{x}{L}-\frac{1}{2})^2} \tag{3.19}$$

while polarization is zero and population inversion is p.

3.2. Finite Difference Formulism for Ring-Cavity with Non-Vacuum Lasing Medium

We can apply the derivation procedure in the last section to the non-vacuum lasing medium characterized by refractive index n. The set of equations with saturable absorber effect in the lasing medium is given by [18]:

$$\frac{\partial \tilde{E}}{\partial t} + \frac{c}{n}\frac{\partial \tilde{E}}{\partial z} = -\frac{c}{n}\tilde{P} - \left(\frac{1}{2}l_0 - \gamma\left|\tilde{E}\right|^2\right)\tilde{E} \tag{3.20}$$

$$\frac{\partial \tilde{P}}{\partial t} = -\frac{1}{2}\tilde{\sigma}\tilde{E} - \frac{\tilde{P}}{T_2} \tag{3.21}$$

$$\frac{\partial \tilde{\sigma}}{\partial t} = \frac{l_0 p}{T_1 T_2} - \frac{\tilde{\sigma}}{T_1} + (2\tilde{E}^*\tilde{P} + c.c.) \tag{3.22}$$

In these equations, c is speed of light, n is the refractive index, T_1 and T_2 are the longitudinal and transverse relaxation times, respectively. The saturable absorber with lowest order approximation in $\tilde{E}$ is presented by γ and the linear loss is l_0. The equations (3.19) explains the propagation of electric field in the medium with loss and varying polarization. Equation (3.20) is the rate of change in the polarization which is a function of magnitude of electric field and inversion.

We have two ways to choose from. One is to write the finite difference equations for each of the variables in equations (3.19)-(3.21) and run the simulation for the new set of equations. The other way is to figure out the correlation between the equations (3.1)-(3.3) and (3.19)-(3.21) and incorporate the conversion coefficients into equations (3.1)-(3.3) with the inclusion of saturable absorber effect. We adopt the second method which is

simpler. By figuring out the correlation between the two sets of equations, the following conversion rules are obtained,

$$T_2 = \frac{1}{\gamma_\perp}$$

$$T_1 = \frac{1}{\gamma_\parallel}$$

$$p = \lambda + 1$$

$$k = \frac{c}{2n}(l_0 - \frac{\mu^2}{\hbar^2}\boldsymbol{\gamma}(2\gamma_\parallel\gamma_\perp\lambda)|E|^2) \tag{3.23}$$

$$\tilde{E} = \sqrt{2\gamma_\parallel\gamma_\perp(p-1)}E$$

$$\tilde{P} = -\frac{l_0}{2}\sqrt{2\gamma_\parallel\gamma_\perp(p-1)}P$$

$$\tilde{\sigma} = l_0\gamma_\perp\sigma$$

So by inserting these coefficients in the finite difference equations (3.2)-(3.4), we can form the new effect of new terms in the equations. The values that are used for the parameters are as follow [18]: gain recovery time, T_1, is 0.5 picoseconds, dephasing time, T_2, is 0.067 picoseconds, and linear cavity loss, l_0, is 500 m^{-1}. The value for refractive index, n_{ref}, is 3.

CHAPTER 4

Results

To run the simulation, MATLAB software with 64-bit operating system and 4 gigabyte memory was used. Obviously, since the equations are nonlinear and coupled, the results are very sensitive to the initial conditions and to the constants that we use in the code. With small change in the amplitude of the initial Gaussian pulse the results would change dramatically. For some cases we had to extend the iteration to higher values so the variables pass the transient state and settle in a stable mode. Therefore, for some of the values we were not able to get the right results because of the limited computer memory or we discarded some of the values because graphs did not make sense.

In order to assure the accuracy of the code, we first verify our results based on our finite difference approximations for equations (3.1)-(3.3) by comparing them with the presented results in Ref. [16]. With the same parameters and initial conditions in Ref. [16], we generated the graph for the intensity versus time. The initial conditions are

$$E(x,0) = 0.1e^{-100(\frac{x}{L}-\frac{1}{2})^2}$$

$$P(x,0) = 0$$

$$\sigma(x,0) = \lambda + 1$$

polarization is chosen to be zero initially because there is no excitation in the medium and inversion is the threshold pumping (the amount of minimum current needed to be injected in the medium so the laser can be started) plus one to give a total pumping.

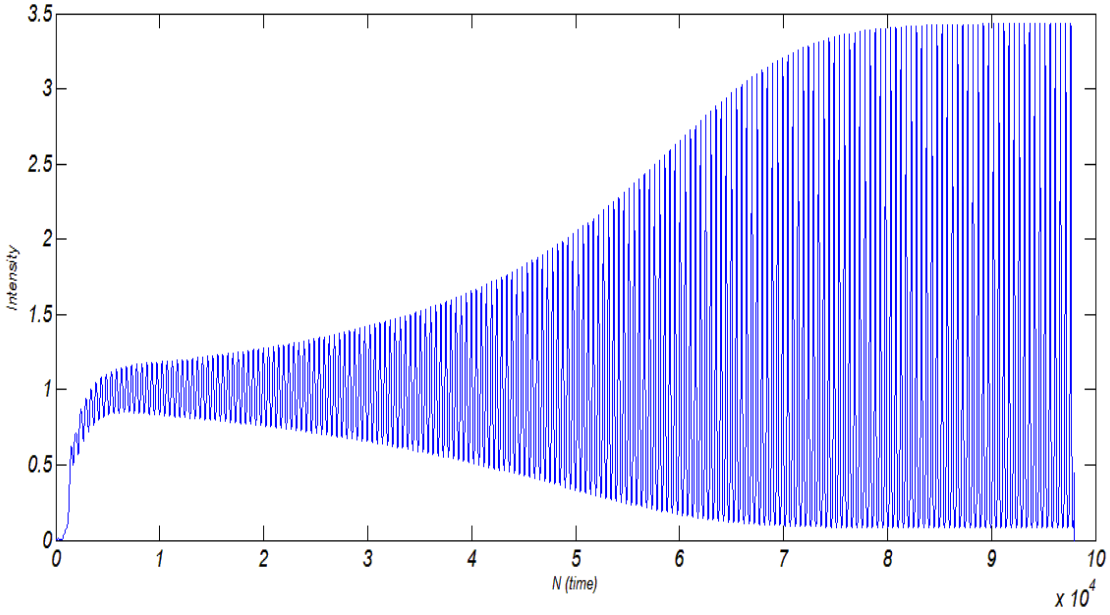

Figure 4-1 Graph of Intensity as a function of time $t = \frac{NL}{c}$ where N is number of trips. In this graph, λ=15, $L = \frac{2\pi c}{3.2\gamma_\perp}$, $k = \frac{1}{10}\gamma_\perp$ and $\gamma_\parallel = \frac{1}{2}\gamma_\perp$. After a few round trips, the variables reach the approximate continuous wave solution. Intensity reaches the stable mode from a Gaussian disturbance.

Figure 4-1 shows transient buildup of the intensity for ring cavity without saturable absorber effect. After a few round trips E, P and σ reach the approximate steady state. This graph agrees with results in Ref. [16].

To investigate the effect of saturable absorber, we change the variables in the code to appropriate counterparts in (3.19)-(3.21) using the conversion coefficients (3.22). In order to compare the results presented in the Ref. [18], we study the optical spectrum of the lasing intensity under various saturable absorber strengths. The optical spectrum is obtained based on Fourier transform of the optical intensity in the time domain and a grid

size of 500×100000 was used which correspond to $\Delta x = 1.2 \times 10^{-5} m$ and $\Delta t = 1.2 \times 10^{-13} s$. We select $\boldsymbol{\gamma}$ value $10^{-11} \frac{m}{V^2}$, which is based on Ref. [18]. We observe optical spectrum of the lasing intensity for various pumping ratio p. The values for p are chosen as 5.0, 5.5 and 5.6 which are above the lasing threshold.

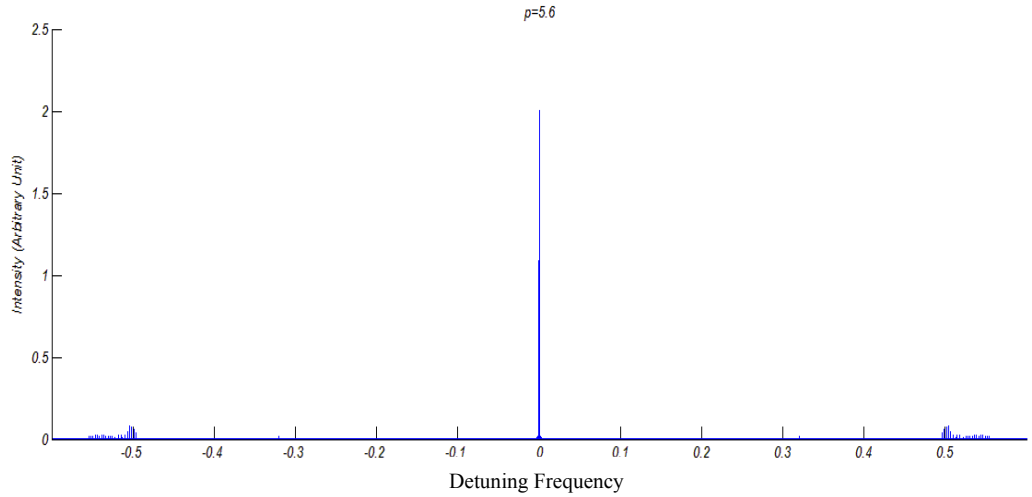

Figure 4-2 Graph of intensity as a function of frequency for $= 5.6$, $\gamma = 10^{-11} \frac{m}{V^2}$. $L = 6\ mm$ to account for round trip with the same time as a $3\ mm$ Fabry-Perot cavity. $l_0 = 700\ m^{-1}$ to account for the mirror losses.

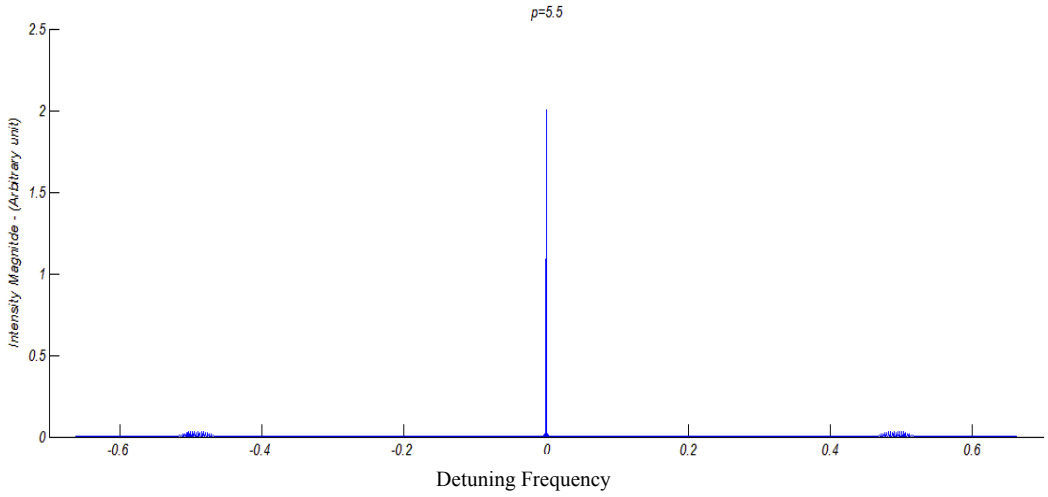

Figure 4-3 Graph of intensity as a function of frequency for $p = 5.5$.

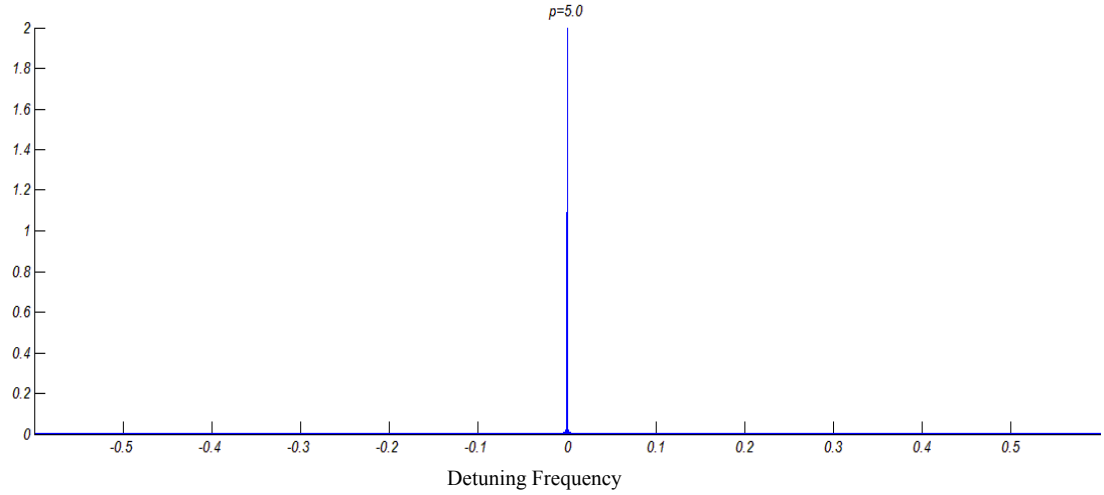

Figure 4-4 Graph of intensity as a function of frequency for $p = 5.0$.

In the three graphs above the spectrum of the pulse is shown. Under the same saturable absorber strength, as the p increases, side peaks around the central peak start to grow. The existence of the side modes is due to the instability of the lasing behavior under higher pumping ratio. The magnitude of variations is better represented in logarithmic graphs. This observation is similar to that presented in Ref. [18].

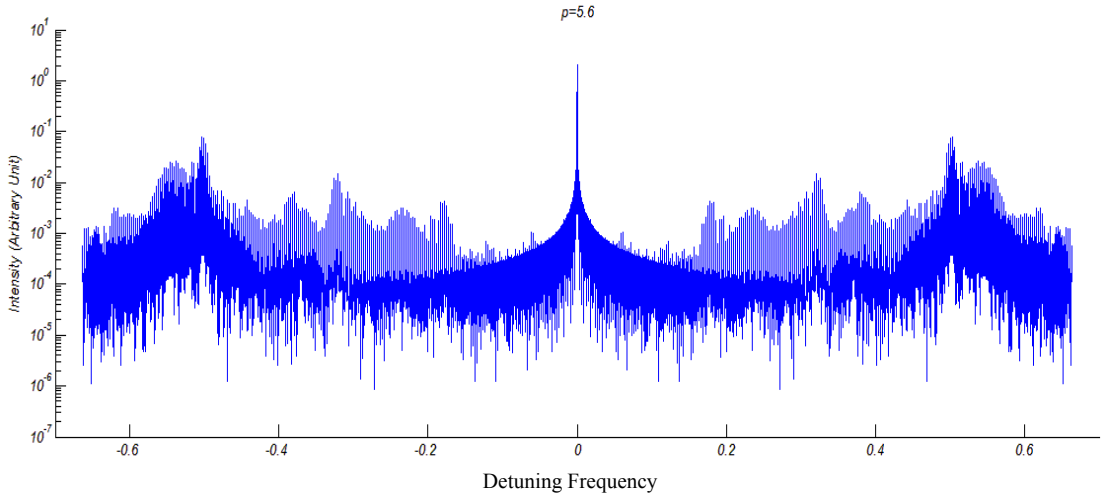

Figure 4-5 Logarithmic graph of intensity as a function of frequency for $= 5.6$, $\gamma = 10^{-11}\frac{m}{V^2}$. $L = 6\ mm$ for round trip with the same time as a $3\ mm$ Fabry-Perot cavity. $l_0 = 700\ m^{-1}$

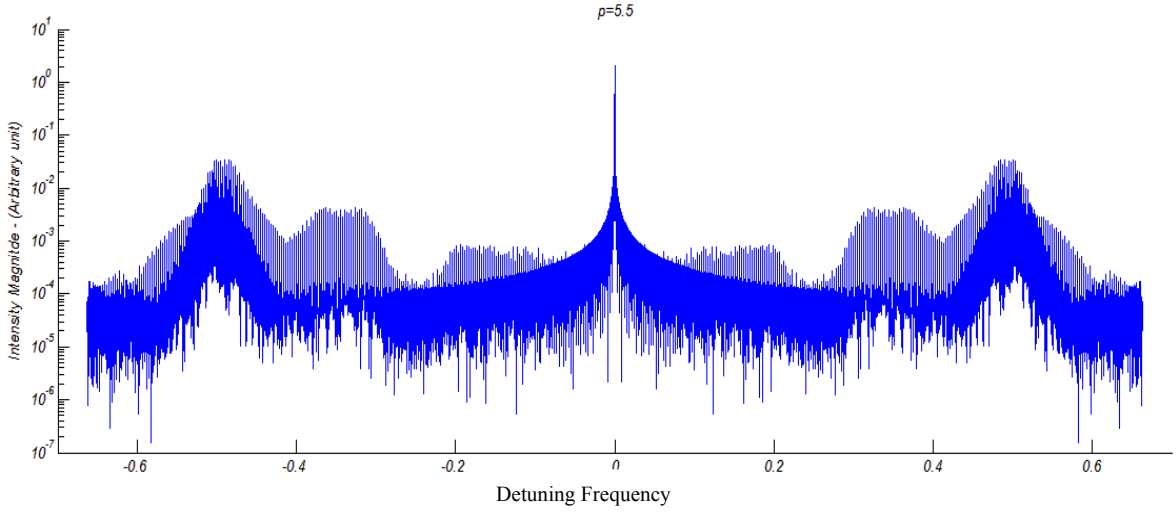

Figure 4-6 Logarithmic graph of intensity as a function of frequency for $p = 5.5$.

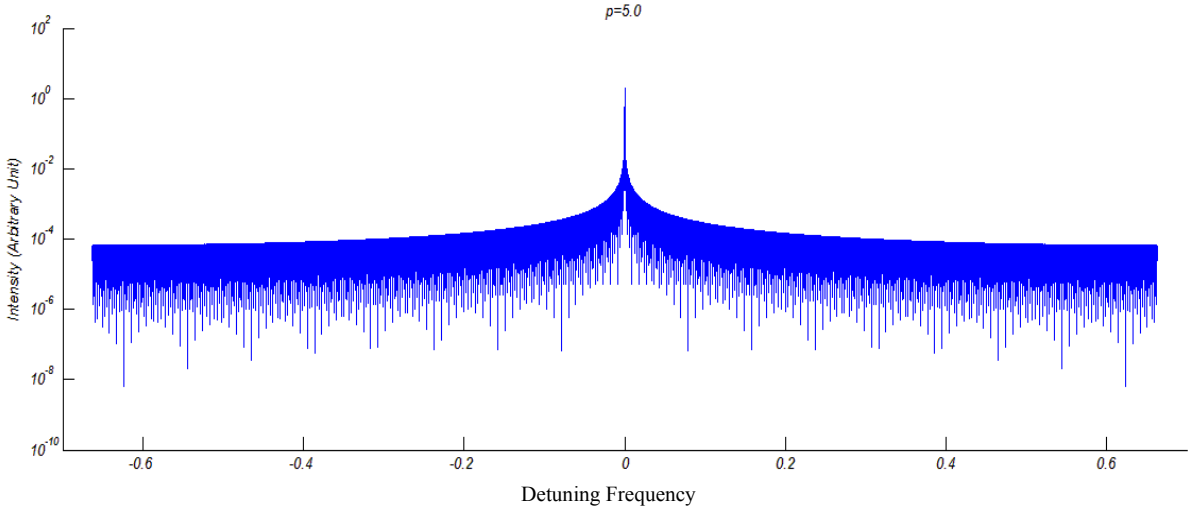

Figure 4-7 Logarithmic graph of intensity as a function of frequency for $p = 5.0$

For □=0, which means no saturable absorber effect, is ignored, we didn't see any change in the optical intensity spectrum under various pumping ratio. This shows that the saturable absorber lowers the threshold of lasing instability. Lasing instability is observed as the rise of the side modes in the lasing spectrum.

CHAPTER 5

Conclusion

In this thesis, we employed a new technique using the correlation relationship to find the finite difference formalism for the Maxwell-Bloch equations for a QCL ring cavity with saturable absorber effect. We performed simulation of optical spectrum based on the formalism derived. We observed the lasing spectrum with influences from the pumping strength and saturable absorber. We found out that the lasing instability, exhibited as the side modes in the optical spectrum, appears with higher pumping ratio under the same saturable absorber effect. Under the same pumping strength, the instability behavior favors the medium with stronger saturable absorber effect. This agrees with conclusion presented in the previous literature.

The derived finite-difference formalism is a favorable numerical method to analyze both static and dynamic behaviors of QCLs. It could be explored to include various physics effects in a QCL medium. In the formalism, the saturable absorber effect is modeled as the intensity-modulated optical field amplitude. Thus, the formalism could also be extended to apply to analysis of the self-phase-modulation effect, which could be described as the intensity-modulated phase of the optical field.

References:

[1] C.Gmachl et al. “Recent Progress in Quantum Cascade Lasers” Rep. Prog. Phys. 64 (2001) 1533–1601

[2] J. Faist et al, “Quantum Cascade Laser” Science, 264 553 (1994)

[3] F. Capasso, “Band-Gap Engineering: From Physics and Materials to New Semiconductor Devices” Science, 235 172-176 (1987).

[4] Sirtori C et al “GaAs/$Al_xGa1_{1-x}As$ quantum cascade lasers” Appl. Phys. Lett. 73 3486–8 (1998)

[5] J. Faist, F. Capasso, C. Sirtori, D. L. Sivco, J. N. Baillargeon, A. L. Hutchinson, S. N. G. Chu, and A. Y. Cho, Appl. Phys. Lett. 68, 3680 (1996).

[6] C.Gmachl , A.Straub , R.Colombelli “ Single-Mode,Tunable Distributed-Feedbackand Multiple-Wavelength Quantum Cascade Lasers.” IEEE JQE 3 569-581 (2002)

[7] H. Kogelnik and C. V. Shank, J. Appl. Phys. 43, 2327, (1972)

[8] C.Gmachl et al, “Continuous-wave and high-power pulsed operation of index-coupled distributed feedback quantum cascade laser” Appl. Phys. Lett. 72, 1430 (1998)

[9] S. Williams, "Terahertz quantum-cascade lasers," Nat. Photonics 1, 517-525 (2007).

[10] Gauthier-Lafaye O et al,’ High-power GaAs/AlGaAs quantum fountain unipolar laser” Appl. Phys. Lett. 74 1537–9 (1999)

[11] J. Bai, “Effect of self-phase modulation on the instabilities of quantum-cascade lasers” Nanophotonics 4, 043519 (2010)

[12] Paiella R et al, “Self-Mode-Locking of Quantum Cascade Lasers with Giant Ultrafast Optical nonlinearities” Science 290 1739–42 (2000)

[13] G. Agrawal, ”Nonlinear Fiber Optics”, Academic Press (2007)

[14] P. Milonni, J. Eberly, “Lasers”, Wiley –Interscience (1998)

[15] H. A. Haus, “Mode-locking of lasers” IEEE J. Sel. Top. Quantum Electron, 6, 1173 (2000)

[16]H. Risken, K. Nummedal, “Self-pulsing in lasers” J. Appl. Phys. 39, 4662 (1968)

[17] L. Casperson, “Rotating-wave approximation in high-gain lasers” Phys. Rev. A, 46 401 (1992)

[18] A. Gordon et al, “Multimode regimes in quantum cascade lasers” Phys. Rev. A, 77 053804 (2008)

[19] Köhler, R. et al. Terahertz semiconductor-heterostructure laser. Nature 417, 156–159 (2002)

[20]http://www.photonics.ethz.ch/research/core_competences/technology/epitaxial_growth/mbe